Aligned Carbon Nanotube Films: Production and Optical and Electronic Properties

Walt A. de Heer,* W. S. Bacsa, A. Châtelain, T. Gerfin,
R. Humphrey-Baker, L. Forro, D. Ugarte

Carbon nanotube material can now be produced in macroscopic quantities. However, the raw material has a disordered structure, which restricts investigations of both the properties and applications of the nanotubes. A method has been developed to produce thin films of aligned carbon nanotubes. The tubes can be aligned either parallel or perpendicular to the surface, as verified by scanning electron microscopy. The parallel aligned surfaces are birefringent, reflecting differences in the dielectric function along and normal to the tubes. The electrical resistivities are anisotropic as well, being smaller along the tubes than perpendicular to them, because of corresponding differences in the electronic transport properties.

Carbon nanotubes (*1–3*), with diameters on the order of 10 nm and lengths over 1000 times their diameters, can now be produced in macroscopic quantities (*2*), which makes them attractive candidates for new materials. These materials are expected to have novel properties. For example, it has been predicted that the cylindrical layers of tubes will be either metallic or semiconducting depending on their diameters (*4*). The testing of these predictions requires well-characterized samples with mutually aligned tubes.

Recently, Ajayan *et al.* (*5*) manufactured a composite such that nanotubes were dispersed in a polymer resin matrix. Slicing the composite caused the nanotubes to align preferentially along the direction of the cut. This work represents an important step, but the rather low tube density, incomplete alignment, and the presence of the resin matrix importantly affect the properties as compared with a pure, aligned material.

We report here a method that can be used to make large surfaces of highly ordered, densely packed carbon nanotubes. We produced the nanotubes using a method described by Ebbesen *et al.* (*2, 3*). A 100-A, 20-V dc arc between a 6.5-mm-diameter graphite anode and a 20-mm graphite cathode is sustained in a 500-torr He atmosphere for ∼20 min. Nanotubes were found on the cathode, where they were encapsulated in a cylindrical shell 1 cm long. The shell was cracked, and the powdery soot-like deposit was extracted. This powder was then ultrasonically dispersed in spectroscopic grade ethanol and centrifuged to remove larger particles. Transmission electron microscopy revealed that the suspension contained nanotubes, nominally 1 to 5 μm long and 10 ± 5 nm in diameter, as determined by transmission electron microscopy of the suspension. However, besides the tubes, we also observed that a substantial fraction of the material was present in the form of small polyhedral carbon particles.

We produced nanotube films by drawing the tube suspension through a 0.2-μm-pore ceramic filter, which left a uniform black deposit on the filter. We then transferred the deposited material onto a plastic surface (Delrin or Teflon) by pressing the tube-coated side of the filter onto the polymer. The filter was lifted off to expose the surface, which was facing the filter. This surface was shiny gray in appearance.

A scanning electron micrograph of this surface is shown in Fig. 1A. There is little evidence of tubular structures; rather, one sees a loose packing of dome-shaped objects, which are much smaller than the pore size of the filter. A remarkable transformation occurs when this surface is lightly rubbed with a thin Teflon sheet or aluminum foil. The surface becomes silvery in appearance, and scanning electron microscopy (SEM) shows that it is densely covered with nanotubes (Fig. 1B), which are oriented along the direction in which the film was rubbed. Hence, we conclude that, for the untreated surface, the tubes are oriented perpendicular to the surface (β-aligned) and that the mechanical treatment pushes them over to lie flat on the surface (α-aligned). The low abundance of polyhedral particles indicates that these particles were probably washed through the filter.

We call the surfaces for which the tubes are oriented in the plane of the surface α-aligned and the surfaces for which they are perpendicular to the surface, β-aligned. Furthermore, $\alpha_{\parallel}$ indicates the direction parallel to and $\alpha_{\perp}$ the direction perpendicular to the tubes, for an α-aligned surface.

The optical properties of these surfaces were measured by ellipsometry with incident angles from 50° to 70° (Fig. 2). We determined the pseudodielectric function $\langle \varepsilon \rangle$ from the measured ellipsometric parameters Ψ and Δ by applying the (air-substrate) semi-infinite model. The α-aligned surfaces are highly anisotropic as revealed by the differences in $\langle \varepsilon \rangle$ when the plane of incidence is along ($\alpha_{\parallel}$) or normal to ($\alpha_{\perp}$) the tube direction, whereas the β-aligned surfaces are optically isotropic. For the α-aligned tubes, we extracted the parallel and perpendicular dielectric functions from the pseudodielectric functions by using a method described by Aspnes (*6*). In con-

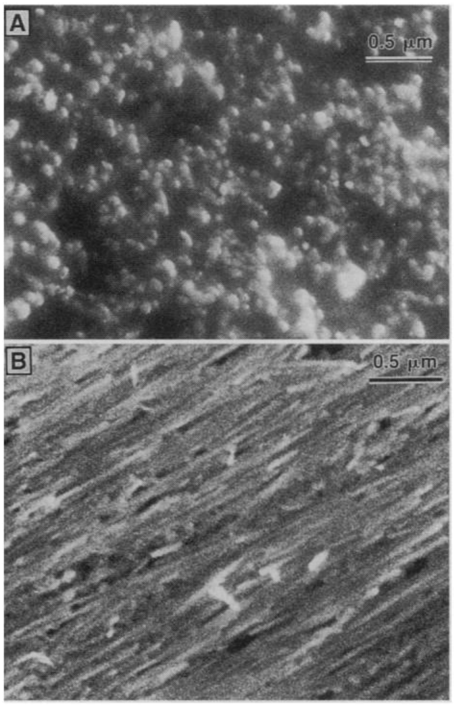

Fig. 1. Scanning electron micrographs of aligned carbon nanotube films. (**A**) The surface of a film of carbon nanotubes deposited on a ceramic filter. The tubes are β-aligned, with their axes perpendicular to the surface so that only the tube tips are seen. (**B**) After mechanical treatment, the morphology dramatically changes and the surface is densely covered with nanotubes that lie flat on the surface and are aligned in the direction in which the surface was rubbed (α-aligned), indicating that the tubes were pushed over by the treatment. The tube tips in (A) appear to be larger than the tube diameters in (B) in part because the tubes are often bundled together and in part because of an artifact caused by focusing and local charging effects (in observations of inclined tubes, the tip images appear brighter and have larger diameters than the tube images).

W. A. de Heer, W. S. Bacsa, A. Châtelain, Institute de Physique Experimentale, Ecole Polytechnique Federale de Lausanne, PHB Ecublens, CH-1015 Lausanne, Switzerland.
T. Gerfin and R. Humphrey-Baker, Institute de Chimie Physique, Ecole Polytechnique Federale de Lausanne, PHB Ecublens, CH-1015 Lausanne, Switzerland.
L. Forro, Institute de Genie Atomique, Ecole Polytechnique Federale de Lausanne, PHB Ecublens, CH-1015 Lausanne, Switzerland.
D. Ugarte, Laboratório Nacional de Luz Síncrotron (CNPq/MCT), Cx. Postal 6192, 13081-970 Campinas SP, Brazil.

*To whom correspondence should be addressed.

trast with the pseudodielectric functions, the derived dielectric functions are almost insensitive to the incident angle, as required. Measurements made on highly oriented pyrolytic graphite (HOPG) for comparison agreed with reported values (*7*).

The ellipsometry results are presented in Fig. 2. The peak at 4.61 eV in $\varepsilon 1$ for the $\alpha_{\parallel}$ case decreases progressively and shifts toward higher energies going to $\alpha_{\perp}$ and β. The shape of the dielectric function for $\alpha_{\parallel}$ is similar to that for HOPG (*8*), whereas for β it is similar to that of glassy carbon (*9*).

We can explain these properties to some extent by noting that for light polarized along the tubes ($\alpha_{\parallel}$), the surface resembles planar graphite (*7*). With light polarized perpendicular to the tubes as in the $\alpha_{\perp}$ case, the dielectric function, from an effective-medium point of view, should look like a mixture of the two dielectric functions of graphite: parallel and perpendicular to the graphitic sheets, that is, $\varepsilon_{gr\perp}$, and $\varepsilon_{gr\parallel}$. This interpretation is consistent with the fact that $\varepsilon_{gr\parallel}$ has a peak at 4.6 eV and $\varepsilon_{gr\perp}$ does not (*10*). The results for the β-oriented surface can be attributed to its complex, nanoscale graphitic morphology (*11*), which in this respect is similar to that of glassy carbon (*9*). Raman cross sections (*12*) of the aligned surfaces, which reveal an enhancement of ~25% in the cross section of the vibrational band at 1582 cm^{-1} for light polarized along the $\alpha_{\parallel}$ direction compared to $\alpha_{\perp}$, indicate a stronger effective photon-phonon coupling in the parallel direction.

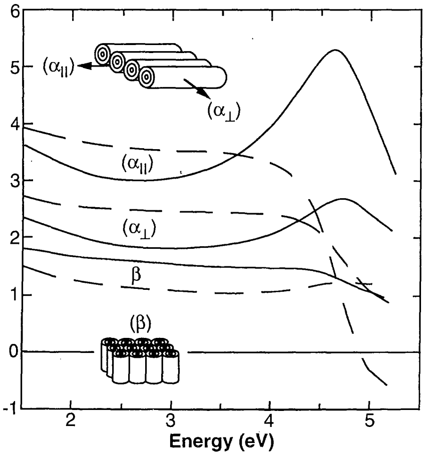

Fig. 2. Dielectric functions of the nanotube films as determined by ellipsometry. The real part of the dielectric function $\varepsilon 1$ is represented with dashed lines, and the imaginary part $\varepsilon 2$ by continuous lines. The α-aligned surfaces are birefringent: In the $\alpha_{\parallel}$ direction the dielectric function resembles that of graphite parallel to the graphitic planes, whereas in the $\alpha_{\perp}$ direction the dielectric function shows features characteristic of the dielectric function of graphite perpendicular to the planes. The dielectric function of the β-aligned surface is isotropic and resembles that of glassy carbon, reflecting similarities between the tube tips and glassy carbon.

We measured the resistivities ρ of α-aligned tubes with the four-contact method both along ($\rho_{\parallel}$) and normal ($\rho_{\perp}$) to the tube direction (Fig. 3). The $\rho_{\perp}$ values are much higher than the $\rho_{\parallel}$ values, and the anisotropy ($\rho_{\perp}/\rho_{\parallel}$) increases with decreasing temperature T. The anisotropy has been measured for samples with several thicknesses. For samples thinner than ~1 μm, the anisotropy is approximately independent of the thickness, indicating that the mechanical procedure aligns the top-1 μm layer of the sample (*13*). The $\rho_{\parallel}$ values measured in our samples are comparable to those recently measured by Langer *et al.* (*14*) in isolated bundles of nanotubes.

We used a variable-range hopping model (*15, 16*) to describe the apparently nonmetallic temperature dependence of $\rho_{\perp}$ and $\rho_{\parallel}$. With this concept one can explain a portion of the anisotropy on the basis of simple geometrical considerations, by assuming that the intrinsic resistance of a tube is much lower than the tube-tube contact resistances. Because fewer tube-tube contacts had to be crossed for a given length of the sample in the $\alpha_{\parallel}$ direction as compared with the $\alpha_{\perp}$ direction, the resistance is lower. However, this explanation fails to account for the very weak T variation (only a factor of 2 in the range from 4 to 300 K) and the temperature dependence of $\rho_{\perp}/\rho_{\parallel}$, especially at low T (<20 K).

We then used a more refined model because the high ρ values and the weak T dependence of ρ are characteristic of a strongly disordered conductor (*17*). Qualitatively, the nanotube material can be thought of as composed of nanoscopic conducting rods. In fact, electron spin resonance measurements show Pauli susceptibility (*18*), indicating that the tubes are metallic. Hence, the high resistivity of the material indicates that strong scattering occurs at the tube boundaries as a result of intertube energy barriers (or disorder potentials) Φ. At high T, $\Phi < kT$ (k is Boltzmann's constant), so that the tube-tube contacts act as static defects, limiting the mean free path of the electrons. The resistivity anisotropy then reflects the mean-free-path anisotropy perpendicular and parallel to the tubes. At low T, when $\Phi > kT$, the energy barriers become more important. The electrons may localize on the individual tubes, and intertube electron transport is thermally activated, requiring electrons to thermally hop across intertube energy barriers (*14*). The strong increase of the anisotropy (for $T < 20$ K) reflects differences in the longitudinal and transverse hopping rates.

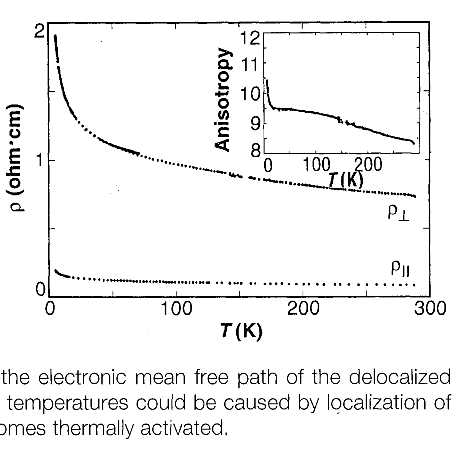

Fig. 3. Resistivities of an α-aligned nanotube film, 5 mm square and approximately 1 μm thick. (Inset) the resistivity anisotropy $\rho_{\perp}/\rho_{\parallel}$. Four parallel, approximately equally spaced silver contact strips were painted on 5-mm-square samples of the nanotube films on Delrin substrates. A current was passed between the outer two electrodes, and the voltage was measured between the inner two electrodes. The resistivities were measured from 4 to 300 K. The resistivity in the $\alpha_{\perp}$ direction ($\rho_{\perp}$) is much larger than in the $\alpha_{\parallel}$ direction ($\rho_{\parallel}$), reflecting analogous effects in crystalline graphite. The high resistivities and their relatively small increase with decreasing temperature are indicative of a disordered conductor whose resistivity is determined by the electronic mean free path of the delocalized electrons. The increase of the resistivities at very low temperatures could be caused by localization of electrons on the tubes so that electron transport becomes thermally activated.

REFERENCES AND NOTES

1. S. Iijima, *Nature* **354**, 56 (1991).
2. T. W. Ebbesen and P. M. Ajayan, *ibid.* **358**, 220 (1992); T. W. Ebbesen, *Annu. Rev. Mater. Sci.* **24**, 235 (1994).
3. T. W. Ebbesen, P. M. Ajayan, H. Hiura, K. Tanigaki, *Nature* **367**, 519 (1994).
4. J. W. Mintmire, B. I. Dunlap, C. T. White, *Phys. Rev. Lett.* **68**, 631 (1992); N. Hamada, S. Sawada, A. Oshiyama, *ibid.*, p. 1579; M. S. Dresselhaus, *Nature* **358**, 195 (1992).
5. P. M. Ajayan, O. Stephan, C. Colliex, D. Trauth, *Science* **265**, 1212 (1994).
6. D. E. Aspnes, *J. Opt. Soc. Am.* **70**, 1275 (1980).
7. E. A. Taft and H. R. Philipp, *Phys. Rev. A* **138**, 197 (1965).
8. In fact, the effective-medium approximation [D. E. Aspnes, J. B. Theeten, F. Hottier, *Phys. Rev. B* **20**, 3292 (1979)], if it is assumed that the surface consists of 60% HOPG and 40% void, reproduces roughly the $\alpha_{\parallel}$ dielectric function. However, neither the $\alpha_{\perp}$ nor the β orientation can be reproduced by this procedure. The dielectric function for the β surface resembles that of glassy carbon: a form of carbon composed of small packets and curved ribbons of graphitic planes with little or no true graphitic orientation between the planes (*7, 9*).
9. M. W. Willams and E. T. Arakawa, *J. Appl. Phys.* **43**, 3460 (1972).
10. See, for example, E. D. Palik, Ed., *Handbook of Optical Constants of Solids II* (Academic Press, Boston, 1991).
11. P. M. Ajayan, T. Ishihachi, S. Iijima, *Chem. Phys. Lett.* **202**, 384 (1993).
12. W. S. Bacsa, D. Ugarte, A. Châtelain, W. A. de Heer, *Phys. Rev. B* **50**, 15473 (1994).
13. The resistivity anisotropies $\rho_{\perp}/\rho_{\parallel}$ at $T = 300$ K vary with the film thickness d as follows: for $d = 8, 4, 2, 1$, and $\ll 1$ μm, $\rho_{\perp}/\rho_{\parallel}$ is, respectively, 1.6, 2.6, 3.4, 8.1, and 6.4.
14. L. Langer *et al.*, *J. Mater. Res.* **9**, 927 (1994).

15. N. F. Mott, *Conduction in Non-Crystalline Materials* (Oxford Univ. Press, New York, 1987).
16. A. W. P. Fung, M. S. Dresselhaus, M. Endo, *Phys. Rev. B* **48**, 14953 (1993).
17. D. Belitz and W. Schirmacher, *J. Phys. C* **16**, 913 (1983).
18. M. Kosuka, T. B. Ebbesen, H. Hiura, K. Tanigaki, *Chem. Phys. Lett.* **225**, 161 (1994).

19. We thank P. Stadelmann and B. Senior of the Interdepartmental Electronmicroscopy Center (EPFL) for use of the Philips EM430 microscope and the SEM work, and A. Janossy, L. Zuppiroli, and R. R. Bacsa for stimulating discussions. This work was supported by the Swiss National Fund.

6 December 1994; accepted 21 February 1995

Phonons Localized at Step Edges: A Route to Understanding Forces at Extended Surface Defects

L. Niu, D. J. Gaspar, S. J. Sibener*

Inelastic helium atom scattering has been used to measure the phonons on a stepped metallic crystalline surface, Ni(977). When the scattering plane is oriented parallel to the step edges and perpendicular to the terraces, two branches of step-induced phonons are observed. These branches are identified as transversely polarized, step-localized modes that propagate along the step edge. Analysis reveals significant anisotropy in the force field near the step edge, with all forces near the step edge being substantially smaller than in the bulk. Such measurements provide valuable information on metallic bonding and interface stability near extended surface defects.

The chemical and physical properties of atomic-level surface defects play a crucial role in governing the outcome of many important interfacial processes such as chemical catalysis (*1–4*) and crystal growth (*5–8*). The vibrational characteristics of steps are particularly informative as they provide direct information on the local force field in the vicinity of such defects. These frequencies also provide a stringent test for electronic structure calculations, which seek to quantitatively explain charge redistribution, structural relaxation, and bonding near extended structural defects. Such information will help us to comprehend more fully the role that such defects play in catalysis, corrosion, interface stability, and crystal growth. Moreover, atomic-level steps provide a physical manifestation of a one-dimensional (1D) system that breaks the symmetry of the surrounding 2D environment.

Several recent studies have examined such issues theoretically (*9–14*), but detailed experimental studies of vibrational dynamics on stepped surfaces have been scarce and preliminary in nature (*15–17*). Of particular relevance to this report are the calculations of Berndt *et al.* (*13*), who predicted the existence of two resonant optical branches on stepped surfaces. The few experiments done so far (*15–17*) show modes at or near the surface Brillouin zone (SBZ) center. For example, only one data point could be assigned as a step-localized phonon (at the SBZ center) on Pt(775) (*15*), and only one step-induced phonon branch was observed for Al(221) (*17*). One would ideally like a much more global determination of the vibrational frequencies of step-localized phonons in order to assess fully the bonding interactions along such extended surface defects.

In this report we discuss our observation of two step-localized transverse surface phonon modes that propagate along steps one atom high on a stepped metallic single crystal, Ni(977). We detected these modes by using energy- and momentum-resolved inelastic neutral He atom scattering. These time-of-flight measurements (which can be viewed as a 2D, surface-sensitive analog to inelastic neutron scattering) were carried out with a high-resolution ultrahigh vacuum scattering instrument (energy resolution, 0.46 meV; angular resolution, 0.36°; chopper-to-crystal distance, 55.1 cm; and crystal-to-ionizer distance, 101.5 cm) (Fig. 1A). A more complete description of the instrument can be found elsewhere (*18*). This technique is particularly well suited for this study as the low-energy He atoms do not penetrate into the bulk; that is, they offer superb discrimination between surface and subsurface phenomena. Moreover, He scattering is more sensitive to steps than electron scattering (*19*).

The best way to prepare a high density of (nearly) identical steps is to intentionally cut a crystal surface a few degrees off from a low-Miller-index plane along a specific azimuthal direction. Such vicinal surfaces contain periodically spaced steps of known density and orientation. The Ni(977) surface used in this study, cut at an angle of 7.02° from the (111) surface plane toward the (2$\bar{1}\bar{1}$) direction, consists of eight-atom-wide (111) terraces that are separated by one-atom-high steps of (100) orientation {in microfacet notation (*20*) Ni[8(111)×(100)]}. The crystal orientation used in these experiments was verified to be within 0.5° of the ideal (977) direction with Laue x-ray back-reflection. We prepared the crystal by repeated cycles of ion sputtering while cycling the crystal temperature between 400 and 1100 K, followed by annealing at 1100 K. We checked surface cleanliness by Auger spectroscopy, with the largest contaminant, sulfur, being reduced in surface concentration to less than 0.1% coverage. Surface order was confirmed with both low-energy electron and He diffraction. We carefully chose the orientation of the scattering plane, aligned parallel to the steps and perpendicular to the terraces (Fig. 1B), to allow us to spectroscopically resolve the desired step-localized phonon modes.

Step-localized phonons are vibrations that are localized to, and propagate along, the step edges of vicinal surfaces. We can develop an understanding of the polarization characteristics of the normal modes associated with step-localized phonons if we think of a step row of atoms as a 1D lattice with a specific orientation in 3D space, similar to phonons propagating along high symmetry directions in cubic crystals (*21–23*). On the basis of this simple picture, there is a longitudinal mode polarized along the step and two orthogonal transverse modes polarized perpendicular to the step. The transverse polarizations are defined by the symmetry of the stepped surface. One is along the macroscopic surface and perpendicular to the steps (the y direction in Fig. 1B), where there is translational symmetry. The other is the normal to the macroscopic surface (the z direction in Fig. 1B).

In order to successfully detect such step-localized phonons, we have had to delineate the "spectroscopic selection rules" that govern the inelastic scattering dynamics; this task is simplified by a judicious choice of scattering geometry. The scattering plane (denoted by S in Fig. 1B) was chosen parallel to the steps and perpendicular to the terraces. The in-plane scattering of He atoms from terraces was used to precisely orient the crystal. A surface lattice vibration will strongly couple with the He beam if the displacement vector of the vibration has an appreciable projection onto the surface normal. Therefore, He scattering will primarily couple to phonon polarizations that have projections onto the surface normal.

L. Niu, James Franck Institute and the Department of Physics, University of Chicago, 5640 South Ellis Avenue, Chicago, IL 60637, USA.
D. J. Gaspar and S. J. Sibener, James Franck Institute and the Department of Chemistry, University of Chicago, 5640 South Ellis Avenue, Chicago, IL 60637, USA.

*To whom correspondence should be addressed.